Sox10 is required for systemic initiation of bone mineralization

Stefani Gjorcheska[1], Sandhya Paudel[1], Sarah McLeod[1], Louisa Snape[2], Karen Camargo Sosa[2], Cunming Duan[3], Robert Kelsh[2], Lindsey Barske[1,4*]

[1]Division of Human Genetics, Cincinnati Children's Hospital Medical Center, Cincinnati, OH, USA

[2]Department of Life Sciences, University of Bath, Bath, BA2 7AY, UK

[3]Department of Molecular, Cellular, and Developmental Biology, University of Michigan, Ann Arbor, MI, USA

[4]Department of Pediatrics, University of Cincinnati College of Medicine, Cincinnati, OH, USA

*Correspondence: lindsey.barske@cchmc.org

Abstract

Heterozygous variants in the gene encoding the SOX10 transcription factor cause congenital syndromes affecting pigmentation, digestion, hearing, and neural function. Most of these symptoms are attributable to failed differentiation and loss of neural crest cells. Extensive research on mouse and zebrafish models has confirmed that Sox10 is essential for most non-skeletal crest derivatives, but seemingly dispensable for skeletal development. We challenge that concept here by revealing a novel requirement for Sox10 in skeletal mineralization. Neither neural crest- nor mesoderm-derived bones initiate mineralization on time in zebrafish *sox10* mutants, despite normal osteoblast differentiation and matrix production. We show that mutants are deficient in the ionocyte subpopulation tasked with taking up calcium from the environment through the Trpv6 epithelial calcium channel, leading to a severe calcium deficit that explains the lack of mineralization. As these ionocytes do not derive from a *sox10*+ lineage, we hypothesized that the primary defect instead resides in a separate organ that regulates ionocyte numbers or

calcium uptake at a systemic level. Screening of the endocrine hormones known to regulate calcium homeostasis in adult vertebrates revealed significantly elevated levels of stanniocalcin (Stc1a), an anti-hypercalcemic hormone, in larval *sox10* mutants. Previous studies demonstrated that Stc1a inhibits calcium uptake in fish by repressing *trpv6* expression and blocking proliferation of Trpv6+ ionocytes. Our epistasis assays indicate that excess Stc1a is the proximate cause of the calcium deficit in *sox10* mutants. Lineage tracing shows that the pronephros-derived glands that synthesize Stc1a interact with *sox10*+ neural crest-derived cells, and that the latter are missing in mutants. We conclude that a subpopulation of Sox10+ neural crest non-cell-autonomously limit Stc1a production to allow the inaugural wave of calcium uptake necessary for the initiation of bone mineralization.

Keywords: Sox10, bone mineralization, neural crest, calcium, stanniocalcin

Introduction

Sry-box transcription factor 10 (SOX10) is essential for pigmentation of the hair and skin, the ability to perceive sound and smell, and for digestive peristalsis. People with only one functional copy of the *SOX10* gene present pigment anomalies such as iris heterochromia and a white forelock, sensorineural hearing loss, deficient enteric innervation, anosmia, neurological abnormalities, neuropathy, and/or stalled puberty[1]. Cases range from mild to potentially lethal and are assigned to one of four congenital syndromes with overlapping clinical features: Waardenburg syndrome types 2E and 4C, Kallmann syndrome, or PCWH (Peripheral demyelinating neuropathy, Central dysmyelination, Waardenburg syndrome, and Hirschsprung disease)[1]. Besides the inner ear and central nervous system phenotypes, these symptoms are largely attributable to failed neural crest (NC) differentiation. This transient, migratory population of embryonic cells gives rise to pigment cells, sensory and enteric neurons and glia, the adrenal medulla, and bone, cartilage, and connective tissues of the facial skeleton[2]. All NC cells (NCCs)

activate *SOX10* expression upon specification, prior to migration. The cranial subpopulation destined to give rise to the facial skeleton turn it off upon reaching their destination in the pharyngeal arches[3,4]. The remaining, non-skeletal NC populations retain Sox10 expression longer to activate programs for differentiation into pigment, glia, and sensory or enteric neurons, among other cell types[5]; in mutants, migration and differentiation stall, and the cells die[6]. Sox10 is also expressed in differentiating chondrocytes of both neural crest and mesodermal origin, but it is not critical there, as cartilage develops normally in zebrafish *sox10* mutants[7]. Accordingly, decades of research on heterozygous patients as well as homozygous mouse and zebrafish models has culminated in the notion that SOX10 is essential for non-skeletal neural crest derivatives but dispensable for formation of the skeleton[6-10].

Bones mineralize by packing an organic collagenous extracellular matrix (ECM) with hydroxyapatite crystals of calcium and phosphate in a highly ordered manner[11]. Mature bone-forming osteoblasts secrete collagen I/X-rich ECM as well as enzymes (e.g. Alkaline phosphatase, Phospho1) and accessory glycoproteins (e.g. Osteopontin, Osteonectin) involved in synthesis and organization of the hydroxyapatite crystals[12-14]. Failed osteoblast maturation, disturbed matrix formation, and calcium-phosphate imbalances can disrupt ossification[15,16].

Endocrine factors, particularly parathyroid hormone, vitamin D, and calcitonin, work in concert to maintain calcium and phosphate homeostasis in adults through actions on bone, intestine, and kidney[17-21]. Adult vertebrates obtain calcium and phosphate for all their cellular needs via dietary sources, environmental uptake, and renal reabsorption, as well as by breaking down bone[22]. However, how the initial wave of calcium and phosphate uptake in the developing embryo is regulated remains a gap in knowledge. Mammalian fetuses obtain minerals largely through the placenta[23], while fish larvae take them from maternal yolk stores or directly out of the water through ionocytes in the skin and gills[24,25]. Indeed, zebrafish larvae obtain the necessary amount

of phosphate through phospholipid metabolism in the yolk and do not require additional environmental phosphate uptake[26-28]. Conversely, calcium uptake from the environment is required for skeletal mineralization[29]. The major route of calcium ingress is the constitutively open epithelial calcium channel (ECaC) encoded by *trpv6* (Transient Receptor Potential channel family, Vanilloid subfamily member 6)[29-31]. Of the five major types of ionocytes in fish, only the Na^+/H^+-ATPase-rich (NaR) subpopulation expresses *trpv6*[25,30]. *Trpv6* expression is also highly enriched in both maternal and fetal cells of the mammalian placenta[32]. Because Trpv6 is constitutively open, regulation of calcium uptake occurs through modulating levels of *trpv6* transcription or the proliferation/quiescence of *trpv6*+ cells[30]. Whether the major endocrine hormones involved in calcium and phosphate homeostasis in adults also control the initiation of calcium uptake via Trpv6 for skeletal mineralization in the embryo remains largely unknown.

One factor known to not drive but rather limit calcium uptake in both embryonic and adult fish is an anti-hypercalcemic hormone called stanniocalcin[33]. Stanniocalcin (Stc1) is a glycoprotein secreted by a variety of tissues in mammals (e.g. kidney, intestine), where it is involved in local calcium homeostasis[34-38]. Stc1a was first isolated from the Corpuscles of Stannius (CS), intermediate mesoderm-derived endocrine organs unique to teleost fish[35,39,40]. Surgical removal of the CS or mutation of the *stc1a* gene causes severe hypercalcemia, kidney stone formation, and an increase in NaR cell numbers in fishes[35,41,42]. Conversely, exposure to high environmental calcium increases *stc1a* mRNA levels and serum Stc1a content, in turn leading to decreased calcium uptake[33]. Stc1a's anti-hypercalcemic activity involves inhibition of both *trpv6* expression and NaR cell proliferation, working through a Pappaa-Igfbp5a-Igf-Igfr cascade that impacts PI3K, mTor, and Akt signaling[42-46]. In normal or low calcium, active Pappaa cleaves the Igf-binding protein Igfbp5a, releasing Igf ligands to activate downstream signaling and NaR cell proliferation. In conditions of high environmental calcium, Stc1a inhibits Pappaa's protease activity, keeping NaR cells quiescent[42-46].

In this study, we present a previously undescribed systemic requirement for Sox10 in the initiation of skeletal mineralization in fish. We provide evidence of a striking Stc1a increase in *sox10* mutants that severely reduces *trpv6*+ ionocyte number and whole-body calcium content. We find *sox10*+ neural crest-derived cells interacting with the Corpuscles of Stannius in control but not mutant fish, indicating that they may serve to moderate *stc1a* levels in the embryo, allowing the massive wave of calcium uptake required to initiate bone mineralization

Results

Delayed onset of skeletal mineralization in zebrafish *sox10* mutants

Though Sox10 expression is activated in all NCCs upon specification[5,6,47,48], it is quickly downregulated in the subset of cranial crest that will go on to form the facial skeleton[4]. These skeletal progenitor cells were presumed to not require Sox10 function, as our early studies noted no defects in the Alcian blue-labeled cartilages of the zebrafish *sox10* mutant facial skeleton[7]. However, while recently performing a routine bone stain in *sox10* mutants, we unexpectedly noticed a striking absence of mineralization when the skeleton is first differentiating at 3-4 days post fertilization (dpf) (Fig. 1A). At these stages, calcium deposits in newly mineralizing bones are readily apparent by Alizarin red staining in sibling controls. Weak staining appears in mutants by 5 dpf and increases until larval lethality around 8 dpf, but never attains control levels. Mutants are not edemic or developmentally delayed, ruling out these common explanations for poor mineralization. The phenotype is also indiscriminate of ossification type (endochondral, intramembranous, and even odontogenic) and bone developmental origin in the mesoderm versus neural crest (Fig. 1B).

As deficient mineralization has not been reported in any of the many existing mouse, fish, or frog Sox10 loss-of-function models, we questioned whether it could be a neomorphism specific to our

sox10^{ci3020} allele[49]. *ci3020* is a 1495-bp deletion that removes part of the 5'UTR and the first coding exon, encoding the homodimerization domain and part of the DNA-binding high mobility group (HMG) domain (Fig. S1A). Some transcription still occurs from the deletion allele[49], and the first in-frame methionine downstream of the deletion could conceivably produce an N-terminally truncated protein lacking the HMG box but retaining the transactivation domain[1]. *sox10*$^{ci3020/ci3020}$ embryos otherwise present the classic *colourless* phenotypes associated with *sox10* loss-of-function (Fig. S1B-C)[50], lacking melanocytes and xanthophores, with malformed otic vesicles and otoliths but normal facial cartilages. To test whether deficient mineralization is specific to the *ci3020* allele, we performed Alizarin red staining on homozygotes for the *m618* (L142Q) missense allele first reported in 1996[51]. The same near-absence of staining was observed between 4 and 6 dpf (Fig. S1D), demonstrating that this phenotype is a general consequence of loss of *sox10* function, at least in zebrafish. We further validated the Alizarin red results in *ci3020* mutants (hereafter *sox10* mutants) using Von Kossa and Calcein stains (Fig. 1C, S1C'), which both label calcium deposits,[52-55] as well as Osteoimage (Fig. 1D), a stain that specifically detects hydroxyapatite[56]. These stains confirmed that mineralization gradually initiates around 5 dpf, first apparent by Von Kossa staining (Fig. 1C). Supporting that the recovery is incomplete, fluorescent Calcein staining in older 7 dpf larvae revealed a lack of endochondral bone collars around the mutant hyomandibula and ceratohyal cartilages (Fig. S1C').

Osteoblasts are essential for mineralization, but do not themselves express Sox10 (Fig. 2A-B)[57]. The subset of osteoblasts derived from the cranial neural crest did transiently express *sox10* and accordingly express the *SOX10:*Cre neural crest lineage label (by a human neural crest-specific *SOX10* promoter)[5,48], but those derived from mesoderm never pass through a *sox10*+ state. We therefore presumed that the broad mineralization deficit would not be cell-autonomous to osteoblasts, though it was still possible that their differentiation could be impacted by extrinsic factors. Osteoblasts are evident as early as 3 dpf at the site of the future opercle (op) bone[58]. To

157 evaluate mutant osteoblasts, we used established transgenic markers *RUNX2*:mCherry[59],
158 *sp7*:EGFP[60] and *osc*:EGFP[29], which are respectively activated in osteoprogenitors and early and
159 maturing osteoblasts. Live imaging of the op bone in *sox10* mutants and sibling controls from 3
160 to 7 dpf revealed seemingly normal patterns for each marker (Fig. 2C-C''). Visualization of
161 *sp7:*GFP in combination with live Alizarin red staining confirmed that individual elements are
162 growing similarly between mutants and controls (Fig. 2D). Colorimetric *in situs* for the major bone
163 ECM component *col10a1a* also revealed normal expression in mutants (Fig. 2E). These findings
164 suggest that mutant osteoblasts are still differentiating and making collagenous matrix despite not
165 being able to mineralize it.
166
167 To determine whether the mineralization machinery is intact in *sox10* mutant osteoblasts, we
168 performed *in situs* and/or semi-quantitative rt-PCR for *phospho1*, *spp1* (Osteopontin), *sparc*
169 (Osteonectin), *alpl* (Alkaline phosphatase), *enpp1*, *entpd5*, *phex*, *fgf23*, *runx2a*, and *runx2b* (Fig.
170 2E, S2)). These genes encode for secreted proteins and enzymes associated with matrix
171 formation, phosphate and calcium regulation, and hydroxyapatite synthesis, in addition to the
172 Runx2 transcription factors required for osteoblast specification. In rt-PCRs performed on cDNA
173 made from pooled 4-dpf embryos, we detected mild increases in *alpl* and *entpd5* in the mutants
174 ($p<0.05$, unpaired t-tests; Fig. S2A). We also observed slight decreases in *spp1*, *phospho1*,
175 *enpp1*, and *fgf23* in the mutants ($p<0.05$, unpaired t-tests; Fig. S2A), a pattern opposite than
176 observed in the zebrafish *enpp1* mutant, which shows increased mineralization[61]. There was no
177 change in *sparc* or *phex*[61] ($p>0.0.5$, unpaired t-tests) in mutant compared to wild-type embryos
178 (Fig. S2A). *In situ* hybridizations revealed unchanged *runx2a* and *runx2b* expression (Fig. S2B),
179 aligning with the live-imaging *RUNX2:*mCherry experiment (Fig. 2D). *spp1* was strikingly reduced,
180 consistent with the rt-PCR result (Fig. S2A-B). However, inconsistent with the rt-PCR results,
181 *phospho1* expression in forming bones appeared largely unchanged in mutant heads (Fig. 2E),
182 while *sparc* appeared reduced (Fig. S2B). Discrepancies may be due to altered expression in

other tissues not captured by the *in situs.* These findings nonetheless demonstrate for the first time that multiple factors linked with mineralization anomalies in animal models and human patients[62-65] are dysregulated in *sox10* mutants.

***sox10* mutants are calcium-deficient**

Disrupted mineral homeostasis caused by mutations in the phosphate regulators *enpp1* and *entpd5* impacts the expression of many other mineralization-regulating factors, including many of the genes we assayed[61,62]. To test whether the observed dysregulation in our mutant could also be a consequence of a systemic mineral imbalance, we measured calcium and phosphate levels in our mutants. As it is not possible to directly measure serum mineral contents in larval fish, we used a colorimetric assay (Fig. 3B) on pooled whole-body samples between 36 and 168 hpf, following standard practice in the field[33,42,66]. In wild-type zebrafish, Ca^{2+} content begins to increase around 3 dpf as the first bones mineralize and continues to rise with age (Fig. 3A)[67]. By contrast, *sox10* mutants had lower Ca^{2+} content compared with controls starting at 3 dpf ($p=0.03$, unpaired t-test; Fig. 3A-B). Consistent with the bone staining in mutants first appearing around 5 dpf (Fig. 1A), we found that mutant Ca^{2+} levels at 5 dpf were approximately equivalent to control levels at 3 dpf (0.01 μg/embryo), suggesting this may be the minimal Ca^{2+} threshold required to initiate mineralization. To further investigate this possibility, we raised wild-type embryos in medium completely devoid of Ca^{2+} and found that mineralization was absent everywhere except the otoliths inside the otic vesicles (Fig. S3A'). These are made of calcium carbonate rather than hydroxyapatite[68,69] and also still form in *trpv6* mutants that cannot take up external calcium[29,30]. The Ca^{2+} content of these wild-type fish raised in 0 mM Ca^{2+} was approximately the same as that of mutants raised in 1 mM Ca^{2+} (Fig. S3A), supporting that this low level is below the threshold needed for bone mineralization. On the other hand, phosphate levels were seemingly unaffected in mutants between 36 and 168 hpf (Fig. S3B), suggesting that lack of calcium is the major cause of the delayed and deficient hydroxyapatite formation (Fig. 1D).

209

210 Other zebrafish mutants with poor mineralization but seemingly normal osteoblasts, e.g., *msp* and
211 *trpv6*, can be rescued by simply increasing the concentration of Ca^{2+} in the media[29,70]. We tested
212 whether this would also improve our phenotype using Ca^{2+} concentrations two- and ten-fold higher
213 than our standard embryo media (2 and 10 mM versus 1 mM, respectively, following[62,70] (Fig. 3C-
214 D)). However, Alizarin red staining at 4 dpf revealed no increase in mineralization in mutants
215 reared in either high-Ca^{2+} medium (Fig. 3D). We then quantified their Ca^{2+} contents at 4 dpf to
216 specifically assess the calcium deficit, finding that mutants raised in the highest-Ca^{2+} environment
217 did show a non-significant increase in Ca^{2+} content, but they remained at a severe deficit relative
218 to controls (Fig. 3D'). Lowering or increasing the phosphate concentration likewise had no impact
219 on mineralization in mutants (Fig. S3C). The mineralization delay in the *sox10* mutants may thus
220 have a more complex etiology than other mutant lines with similar phenotypes.

221

222 Calcium is taken up from the environment in fish larvae through Trpv6 channels present on the
223 surface of specialized NaR ionocytes in the skin[71]. NaR cells also uniquely express *igfbp5a*[44,72]
224 and comprise a subset of ionocytes expressing Na^+/K^+ ATPase[25]. Immunostaining for Na^+/K^+
225 ATPase combined with the *SOX10:*Cre lineage label (driven by a human neural crest-specific
226 enhancer[5,48]) in otherwise wild-type fish confirmed that these skin ionocytes do not derive from
227 neural crest (Fig. 4A), in line with previous work tracing them to the ectoderm[73]. We questioned
228 whether the persistently low calcium content of *sox10* mutants could be due to a deficiency of
229 *trpv6* expression or total NaR ionocytes. Though rt-PCR revealed no overt change in whole-body
230 *trpv6* levels (Fig. 4B), we did detect significant decreases in the numbers of *trpv6*+ and *igfbp5a*+
231 cells at 4 dpf, with mild recovery by 7 dpf (Fig. 4C-D'). These patterns support reduced NaR
232 number (rather than *trpv6* transcription) as the cause of the systemic calcium deficit and the
233 associated lack of bone mineralization. Published scRNAseq data confirm that differentiating NaR

cells contain no *sox10* transcripts[74]. The NaR deficit in *sox10* mutants therefore cannot be explained by a simple cell-autonomous requirement for Sox10.

NaR cell numbers fluctuate depending on the amount of calcium in the environment, with low Ca^{2+} stimulating their proliferation and thereby increasing Ca^{2+} uptake, versus minimal proliferation and uptake under high Ca^{2+} [24,75]. These fluctuations still occur in *sox10* mutants (Fig. S4A), indicating that they are still capable of responding to environmental conditions. However, the increase in NaR cells observed in mutants raised at low Ca^{2+} is dampened relative to controls, apparently insufficient to raise total Ca^{2+} content (Fig. S3A) or permit robust skeletal mineralization (Fig. S3A').

Endocrine suppression of NaR ionocyte expansion in *sox10* mutants

The fact that the number of *trpv6*+ NaR cells remains so low in *sox10* mutants despite their clear need for calcium struck us as paradoxical. We reasoned that mutants might be lacking a factor needed to stimulate NaR proliferation, or, conversely, have too much of a different factor that blocks their increase. In an rt-PCR screen of candidate endocrine factors, we identified stanniocalcin-1a (*stc1a*) as being 3-fold upregulated in *sox10* mutants at 4 dpf (Fig. 5A). Stc1a is an anti-hypercalcemic hormone triggered by high environmental calcium through activation of the Calcium-Sensing Receptor (CaSR)[33,76-78]. Stc1a reduces calcium uptake to maintain physiologically safe levels by inhibiting proliferation of NaR cells and suppressing *trpv6* expression[42,45]. The dominant sources of Stc1a in fish larvae are the Corpuscles of Stannius, teleost-specific glands that bud off the distal pronephros by 50 hpf and are positioned to either side of the posterior cardinal vein with their own vascular supply by 3 dpf (Fig. 6A-B)[40,79,80]. *stc1a* expression is detectable prior to completion of CS extrusion[40] and is thus potentially involved in maintaining calcium balance as early as 24 hpf[40].

Aberrantly elevated *stc1a* expression in *sox10* mutants might thus explain their reduced number of NaR cells and calcium uptake. In situ analyses showed that the robust increase first becomes apparent after completion of CS extrusion (after 36 hpf; Fig. 5C), is most obvious at 4 dpf (Fig. 5B-C), then begins to level out by 7 dpf (Fig. 5C), when both *trpv6*+ NaR cell numbers and mineralization are partially recovering. The *stc1a* increase is due at least in part to higher numbers of *stc1a*+ cells in the mutant CS between 45 hpf and 4 dpf ($p<0.001$, unpaired t-test; Fig. 5D). Interestingly, in low-Ca^{2+} medium, *stc1a* expression is undetectable in controls but merely reduced in mutants (Fig. S4B), possibly explaining why mutants still have fewer NaR cells and less calcium uptake than their siblings under these conditions (Fig. S3A, S4A).

The *stc1a*-expressing Corpuscles are derived from intermediate mesoderm[40,81] and never pass through a *sox10*+ state, so their dysfunction in *sox10* mutants must also be indirect. We looked for *sox10* lineage+ cells in or surrounding the glands, predicting that they may be aberrant or missing in mutants. We tracked neural crest using *SOX10*:Cre[5,48] in combination with the *actb2:*BFP>DsRed Cre reporter[82] and all recently *sox10*-expressing cells using *sox10*:DsRed (driven by the 4.9-kb zebrafish *sox10* promoter[83]). All traces were performed in combination with the *Tp1:*VenusPEST Notch reporter[84] or the *her6:*mCherry reporter[85], both of which are expressed in the CS after ~36 hpf. We detected a close physical interaction between *sox10:*DsRed+ cells and the CS as early as 50 hpf (Fig. 6C), after the glands had fully formed. The closest cells appear to turn off *sox10* shortly thereafter, as they became harder to find, though lineage-traced crest were present in the vicinity of the CS up to 7 dpf (Fig. 6D-E). Strikingly, *sox10* mutants lack *SOX10*:Cre lineage-labeled cells around the CS at all stages examined (Fig. 6D-E). This is consistent with the complete or near-complete loss of many neural crest cell sublineages previously reported in *sox10* mutant models[6,7,86]. Mutant VenusPEST+ CS cells are less organized, and mutant gland volume is larger ($p<0.0001$ at 58 and 72 hpf, $p=0.003$ at 96 hpf, ns at 168 hpf; unpaired t-tests; Fig. 5E'). These patterns suggest that *sox10*+ crest-derived cells may

act locally to restrain CS growth and *stc1a* expression to regulate embryonic calcium homeostasis.

***stc1a* is epistatic to *sox10* and the proximate cause of the mineralization deficit**

Our results thus far suggested that the absence of *sox10*+ cells leads to unrestrained growth and Stc1a production by the Corpuscles, in turn inhibiting NaR cell proliferation and preventing sufficient calcium uptake for mineralization. To test this model, we performed an epistasis assay of *stc1a* on the *sox10* mutant background using the previously reported *stc1a*^{mi610} mutant[42]. *sox10*^{ci3020}*; stc1a*^{mi610} double mutants present both the trademark lack of pigmentation and underdeveloped inner ears of *sox10* single mutants alongside the characteristic cardiac edema of *stc1a* mutants (Fig. 7A), supporting that these phenotypes are genetically independent. However, bone mineralization was strikingly improved in double mutants relative to *sox10* single mutants at 4 dpf (Fig. 7B). Eighty percent of the double mutants (24 out of 30) stained with Alizarin red: 13 weakly, 10 intermediate, and 1 strongly (Fig. 7E, also see Fig. S5B for examples). It is worth noting that the presence of cardiac edema in the double mutants may have compromised bone formation in some individuals. For comparison, among 23 *sox10*$^{-/-}$*; stc1a*$^{+/+}$ individuals, 14 had no staining, 5 had weak staining, 3 intermediate, and 1 strong (Fig. S5B; p=0.0206, Chi-square test). In the original *sox10*^{ci3020} single mutant crosses, only 3/48 single mutants showed intermediate or weak staining; the other 45 had none (Fig. S5A), suggesting the presence of genetic modifiers. We further noted significant improvement in NaR cell number and calcium content in the double *sox10; stc1a* mutants relative to *sox10* single mutants (Fig. 7C'-D), further supporting that *stc1a* is epistatic to *sox10* in mineral regulation.

Discussion

Novel Sox10 requirement in bone mineralization

This study challenges the decades-old paradigm that Sox10 is not required for skeletal development by revealing a previously undescribed, indirect role in mineralization. Two independent *sox10* mutant lines exhibit delayed and reduced mineralization of all bones, no matter their embryonic origin or ossification type. Mutant osteoblasts appear to differentiate normally (Fig. 2D) and gradually lay down ECM to create typically-sized bone templates (Fig. 2C-E). However, their transcriptomes may be subtly altered: we detected changes in whole-body mRNA levels of genes encoding osteoblast-enriched enzymes involved in regulation of phosphate availability and homeostasis (*phospho1*, *alpl*, *enpp1*, *entpd5*) or bone accessory proteins (*spp1* (osteopontin) (Fig. S2A-B). We posit that these shifts may reflect secondary transcriptional responses of osteoblasts to the major systemic calcium deficit or to changes in inorganic phosphate availability incurred by the lack of calcium. Reduced levels of some of these factors may exacerbate the mineralization defect in *sox10* mutants, as other studies have demonstrated that partial or complete genetic loss of some of these accessory proteins and enzymes can lead to decreased bone mineral density and/or mineralization deficits[62-65].

We noted with interest the changes in phosphate regulators, given that we did not measure any consistent differences in mutants' total phosphate content by a colorimetric assay (Fig. S3B). It is possible that the assay is insufficiently sensitive or overwhelmed by maternally deposited yolk stores[26-28]. However, how osteoblast-engendered inorganic phosphate intended for hydroxyapatite formation is managed when calcium is not available is an intriguing question. Of note, in our comparison of bone stains, we observed recovery of Von Kossa staining before that of Alizarin red, Calcein, or OsteoImage (hydroxyapatite). In Von Kossa staining, silver cations from the silver nitrate staining solution interact with calcium phosphate to produce a yellowish silver phosphate, which subsequently blackens surrounding organic matter[52,87,88]. It is possible that the early recovery of this stain reflects a reaction with inorganic phosphate accumulating in the bone matrix due to the calcium deficit.

How calcium uptake and bone mineralization begin to recover in *sox10* mutants is still an open question. One possibility is that other endocrine hormones come 'online' and begin to counteract elevated Stc1a activity. Parathyroid hormone and vitamin D are reported to have hypercalcemic properties in fish as well as in mammals, acting to increase Trpv6-mediated calcium uptake[21,89,90]. Zebrafish lack parathyroid glands, but express parathyroid hormones in the central nervous system and sensory neuromasts[91]. Similarly, fish synthesize vitamin D as early as 3 dpf in response to decreased environmental calcium[89]. Other physiological changes are occurring in fish larvae at the same time that mineralization begins to recover, including maturation of the digestive tract and auxiliary endodermal organs[92] and depletion of the yolk[26]. Though *sox10* mutants lack an enteric nervous system[7] and are not fed in our experiments, it is possible that passage of embryo medium through the digestive tract allows calcium uptake through intestinal enterocytes, contributing to the mutants' partial recovery. We have also observed ectopic calcium/hydroxyapatite deposits in the yolk area of mutants at 3 and 4 dpf that begin to resolve coincident with the onset of bone mineralization (Fig. 1C-D). The calcium in those deposits could conceivably be remobilized and made available for forming bones as the yolk is depleted. Two other zebrafish mutants that lack mineralization during larval stages (*msp*[70], *her9*[58]) also naturally recover to some extent, supporting robustness or complementarity in mechanisms driving calcium uptake for skeletal mineralization.

Sox10 drives bone mineralization indirectly through interactions with endocrine glands involved in calcium homeostasis

The most striking finding from the whole-body transcriptional analysis was the tripled *stc1a* mRNA levels in *sox10* mutants (Fig. 5A). High Stc1a blocks proliferation of *trpv6*+ ionocytes[42], reducing calcium uptake. That elevated *stc1a* is the major driver of the calcium deficit in *sox10* mutants was confirmed by our epistasis studies (Fig. 7). However, whether the increase in *stc1a* mRNA is

363 attributable solely to the higher cell number in the mutant Corpuscles (Fig. 5C-D) or also to a per-
364 cell increase in transcription is not yet clear. Previous studies have shown that high external
365 calcium upregulates *stc1a* transcription at least in part via the Calcium-Sensing Receptor (CaSR),
366 which is also expressed in the CS[77]. Aberrant activity of CaSR in the absence of *sox10*+ lineage
367 cells could therefore potentially boost *stc1a* transcription. In support of the idea that the *stc1a*
368 increase is more complex than just increased CS cell number, another mineral-regulating
369 hormone enriched in the CS, *fgf23*[93,94], is downregulated in *sox10* mutants (Fig. S2A) despite the
370 increased size of the Corpuscles. Fgf23 has anti-hypercalcemic effects similar to Stc1a, reducing
371 Ca^{2+} uptake in conditions of high systemic calcium, in addition to regulating phosphate
372 homeostasis[77,95,96]; its low expression in *sox10* mutants is consistent with their calcium deficit[77].
373 Published scRNAseq data[74] shows that Corpuscle cells also express receptors for other
374 endocrine factors involved in mineralization between 2 and 4 dpf, including receptors for calcitonin
375 (*calcr*), cortisol (*nr3c1*), vitamin D (*vdrb*), Fgf23 (*fgfr1b*), and Msp (*mst1rb*). It remains to be seen
376 how these pathways are affected in the absence of *sox10*+ cells and whether they are involved
377 in *stc1a* upregulation.
378
379 Why the Corpuscles, derived from a *sox10*-negative mesodermal lineage, are so profoundly
380 affected by loss of *sox10* is not fully resolved. We did not observe an increase in *stc1a*+ cell
381 number before 2 dpf, i.e., only after the glands had fully extruded from the pronephros, ruling out
382 expanded CS specification as the explanation for the larger glands (as previously found in other
383 mutant lines[80,97]). Our experiments instead revealed that a *sox10*+ sublineage interacts with these
384 glands post-extrusion, and that these NC-derived cells are missing in *sox10* mutants (Fig. 6C-E),
385 like so many other crest derivatives[6-9]. A tantalizing possibility is that they may be precursors of
386 the sympathetic neurons that will innervate the CS in adults[79,98]. Sympathetic neurons derive from
387 *sox10*+ neural crest, in particular from Schwann cell precursors (SCPs)[99]. Differentiating Schwann
388 cells and SCPs are thought to be the predominant *sox10*+ cell types lining the trunk sensory and

motor axon tracts that pass by the Corpuscles[3,99], from which we see cells emerging to contact the glands directly (Fig. 6C). Schwann cells and SCPs are largely absent in *sox10* mutant fish and mice[7,10]. Interestingly, hallmark signs of sympathetic neuronal differentiation in the trunk are not evident in wild-type zebrafish until around 7 dpf[100], well after this CS phenotype arises. The regulatory interaction between the *sox10*+ lineage cells and the CS is thus expected to be non-neuronal in nature at these early stages. Though mutant lethality makes it challenging to study the onset of sympathetic control, we expect that the requirement for *sox10*+ lineage cells in managing stanniocalcin production and/or secretion and thus calcium homeostasis persists throughout the lifespan.

Humans and other mammals do make stanniocalcin hormones, but we do not develop a gland homologous to the Corpuscles of Stannius[35]. If loss of *sox10* in fish impacts mineralization solely through dysregulation of Corpuscle development and function, as our data support, it is conceivable that mammals lacking *Sox10* will show no equivalent signs of mineral dysregulation. However, our studies also prompt the more general notion that crest-derived cells destined to become part of the sympathetic nervous system may make contact with and begin regulating their target organs' growth and activity earlier in embryonic development than previously appreciated. This could potentially drive physiological and endocrinological symptoms in individuals with congenital neurocristopathies caused by deficient crest production or survival[101].

Materials & Methods

Zebrafish husbandry and lines

Zebrafish embryos were grown at 28.5°C in standard embryo medium (EM) [102] unless otherwise noted: 15 mM NaCl, 0.5 mM KCl, 1 mM $CaCl_2$•$2H_2O$, 0.15 mM KH_2PO_4, 0.06 mM NaH_2PO_4 and 1 mM $MgSO_4$•$7H_2O$. Published mutant and transgenic lines used here include *sox10*^{ci3020} [49] *sox10*^{m618} [51], *stc1l*^{mi610} [42], *Tg(Hsa.RUNX2:mCherry)*^{zf3244} (alias *RUNX2:mCherry*)[59],

Tg(sp7:EGFP)^{b1212} [60], *Tg(Ola.Bglap:EGFP)*^{hu4008} (alias *osc:EGFP*) [29], *Tg(Mmu.Sox10-Mmu-Fos:Cre)*^{zf384} (alias *SOX10:Cre*) [48], *Tg(EPV.TP1-Mmu.Hbb:Venus-Mmu.Odc1)*^{s940} (alias *Tp1:VenusPEST*) [84], *Tg(fli1:EGFP)*^{y1} [103], *Tg(Xla.Eef1a1:loxP-DsRed2-loxP-EGFP)*^{zf284} (alias *ef1a:DsRed>EGFP*) [48], *Tg(actb2:LOXP-BFP-LOXP-DsRed)*^{sd27} (alias *actb2:*BFP>DsRed) [82] and *Tg(her6:mCherry)*^{sd64} [85]. Lines were maintained as hetero- or hemizygotes.

Bone staining

For all fixed bone stains, zebrafish larvae were fully anesthetized with MS-222 (aka Tricaine, Syndel, USA) at the desired stage and then fixed in 2% paraformaldehyde (PFA) (250 μl embryo medium, 250 μl 4% PFA, and 500 μl PBS with 0.1% Tween) overnight at 4°C or for 1 hour at room temperature. For Alizarin red-only staining, following fixation, larvae were rinsed twice in 25% glycerol in 0.5% KOH for 10 minutes each and stained with 0.01% Alizarin in 25% glycerol/100 mM Tris pH 7.5 for 4 hours at room temperature. They were then bleached for 10 minutes in 3% H_2O_2 in 0.5% KOH under a light source. Specimens were stored and imaged in 50% glycerol in 0.5% KOH or 100% glycerol immediately to prevent fading (adapted from[104]). Combined Alcian blue and Alizarin red staining was performed as described previously[105]. For Von Kossa staining, fixed embryos were rinsed with deionized water and stained with 2.5% silver nitrate solution (Abcam ab150687) under a light source for 20 minutes. The reaction was stopped with 5% sodium thiosulfate to prevent overstaining, and larvae were imaged immediately[106,107]. For the Osteoimage™ Mineralization Assay (Lonza PA-1503), we followed the manufacturer's protocol after fixing. Briefly, fixed larvae were rinsed with diluted wash buffer then stained in diluted Staining Reagent for 30 minutes at room temperature in the dark. Before imaging, they were rinsed three times with wash buffer for five minutes each. For live staining, larvae were incubated in Alizarin red (0.03 mg/ml in 30 ml EM) for 2 hours at 28.5°C or in Calcein green (0.1 mg/ml in

30 ml EM) at 28.5°C overnight[55]. For each round of each bone staining experiment, a minimum of six individuals were stained and imaged per genotype/stage/group.

Calcium and phosphate supplementation and depletion treatments

For calcium treatments, the amount of $CaCl_2$•$2H_2O$ was increased two or ten-fold for 2 mM and 10 mM treatments, respectively, completely removed (0 mM), or decreased to 0.02 mM[70]). For the high phosphate treatment (adapted from [62]), the concentrations of KH_2PO_4 and NaH_2PO_4 were raised to 0.5 mM and 9.5 mM, respectively, to increase the total PO_4^{3-} to 10 mM, therefore maintaining the proportional K^+/Na^+ ratio as in the control EM. The 'No PO_4^{3-}' treatment included neither KH_2PO_4 nor NaH_2PO_4 in the media. A minimum of six control and six mutant larvae were used per treatment group, and all treatments were repeated at least twice.

Whole mount in situ hybridization and immunostaining

cDNAs for *stc1a*, *trpv6*, *igfbp5a, col10a1a*, *phospho1, sparc, spp1, runx2a, and runx2b*[108] were amplified by Herculase II Fusion DNA Polymerase (Agilent) (see Table S1 for primer sequences) and inserted into the pCR-Blunt II-TOPO vector (ThermoFisher). After sequence confirmation and linearization by restriction digest, antisense probes were synthesized from each plasmid using Sp6 or T7 polymerase and digoxigenin (DIG)-tagged nucleotides (Roche). Colorimetric and fluorescent *in situ* hybridizations were performed as described previously[109]. Colorimetric *in situs* were developed with either NBT-BCIP or BM Purple (Sigma-Aldrich), whereas fluorescent *in situs* were developed with TSA Cyanine 3 (Akoya Biosciences). Immunostaining was performed as described[49]. Primary antibodies included anti-Na^+/K^+ ATPase (1:400, DSHB α5) and anti-Sox10 (1:500, Genetex GTX128374), used with AlexaFluor 647-conjugated goat anti-mouse and donkey anti-rabbit secondary antibodies (1:250, ThermoFisher A32728 and B40956). In both procedures, permeabilization steps were skipped for markers limited to surface expression (*trpv6, igfb5a* and

α5). A minimum of six control and six mutant larvae were stained and imaged for each marker, and the experiments were repeated at least twice.

Semi-quantitative reverse-transcriptase PCR (rt-PCR)

rt-PCRs were performed to estimate transcript levels of mineralization-associated genes in *sox10*^{ci3020} mutants. Each sample consisted of 10-15 mutant and 10-15 stage-matched wild-type controls that were pooled at 4 dpf and frozen at -80°C. RNA was extracted using the RNAqueous-4PCR Total RNA Isolation Kit (Invitrogen), and equivalent amounts were used to synthesize cDNA with the High-Capacity cDNA Reverse Transcription Kit (Applied Biosystems). rt-PCR was run with a minimum of three biological replicates per genotype, and *eef1g* expression was used for normalization (following [49]). Band intensity was quantified with Image Lab (BioRad) and analyzed with Prism 10 (GraphPad). Primers, product sizes, and cycling conditions for each gene are listed in Table S2.

Quantification of mineral content

Whole-body Ca^{2+} and PO_4^{3-} contents were quantified using colorimetric assay kits (Abcam ab102505 and ab65622). For Ca^{2+} measurements, 10-15 larvae were pooled at the desired stage in an Eppendorf tube without any liquid, dehydrated at 60°C for 1 hour, then digested for at least 4 hours in 125 µL of freshly prepared 1M HCl in an Eppendorf Thermomixer set at 95°C and 750 rpm. The samples were then centrifuged at 4°C for 45 minutes at 15,000 rpm. Supernatants were distributed on a clear 96-well polystyrene flat-bottomed plate alongside the standard curve reagents prepared according to the protocol provided with the kits. Absorbances were measured on a SpectraMax M5 plate reader. The same procedure was followed for PO_4^{3-} quantification, with the modification that the supernatants were diluted in deionized water to avoid precipitation.

Imaging and image analysis

Skeletal stains, brightfield images and colorimetric *in situs* were imaged on a Zeiss SteREO Discovery.V8 or Zeiss Axioimager.Z1 microscopes, whereas fluorescent *in situs*, fluorescent bone stains, live transgenic fish, and immunostained specimens were imaged on a Nikon C2 confocal. *trpv6+/igfbp5a+* ionocytes and *stc1a+* cells were quantified using the 'spots' option in Imaris 10.1.1. CS volumes were measured with the surface labeling option in Imaris 10.1.1. A minimum of six replicates were counted for each genotype/stage combination.

Data analysis

Data analysis was performed with GraphPad Prism (Version 10.2.3). p-values were calculated with Chi-square tests or unpaired two-tailed t-tests as noted in the figure legends.

Acknowledgments

We are grateful to members of the Barske lab for helping with molecular biology experiments and imaging; Kristina Preusse and Benjamin Liou for assistance with mineral quantification; Evan Brooks and Samantha Brugmann for helping to set up Von Kossa and OsteoImage staining; Colin Kenny, Chunyue Yin, Claire Arrata, and Gage Crump for sharing fish lines; Flynn Littleton, Eric Alley and the CCHMC Division of Veterinary Services for fish care; and Josh Gross, James Nichols, Jessica Nelson, and Rolf Stottmann for helpful discussions and/or manuscript suggestions. Funding for this project was provided to L.B. by Cincinnati Children's Center for Pediatric Genomics and the Cincinnati Children's Research Foundation; funding for L.S. and K.C.S. was provided by BBSRC grant BB/S015906/1 to R.N.K.

Author Contributions

The project was conceived by S.G. and L.B. Zebrafish experiments were performed by S.G., S.P., S.M. L.S., K.C.S., and L.B. Crucial fish lines and guidance were provided by C.D. and R.K. Writing and interpretation were performed primarily by S.G. and L.B. with input from C.D. and R.K.

Reference List

1. Pingault, V., Zerad, L., Bertani-Torres, W. & Bondurand, N. SOX10: 20 years of phenotypic plurality and current understanding of its developmental function. *J Med Genet* **59**, 105-114 (2022).
2. Martik, M.L. & Bronner, M.E. Regulatory Logic Underlying Diversification of the Neural Crest. *Trends Genet* **33**, 715-727 (2017).
3. Kuhlbrodt, K., Herbarth, B., Sock, E., Hermans-Borgmeyer, I. & Wegner, M. Sox10, a novel transcriptional modulator in glial cells. *J Neurosci* **18**, 237-50 (1998).
4. Blentic, A. *et al.* The emergence of ectomesenchyme. *Dev Dyn* **237**, 592-601 (2008).
5. Antonellis, A. *et al.* Identification of neural crest and glial enhancers at the mouse Sox10 locus through transgenesis in zebrafish. *PLoS Genet* **4**, e1000174 (2008).
6. Dutton, K.A. *et al.* Zebrafish colourless encodes sox10 and specifies non-ectomesenchymal neural crest fates. *Development* **128**, 4113-25 (2001).
7. Kelsh, R.N. & Eisen, J.S. The zebrafish colourless gene regulates development of non-ectomesenchymal neural crest derivatives. *Development* **127**, 515-25 (2000).
8. Herbarth, B. *et al.* Mutation of the Sry-related Sox10 gene in Dominant megacolon, a mouse model for human Hirschsprung disease. *Proc Natl Acad Sci U S A* **95**, 5161-5 (1998).
9. Southard-Smith, E.M., Kos, L. & Pavan, W.J. Sox10 mutation disrupts neural crest development in Dom Hirschsprung mouse model. *Nat Genet* **18**, 60-4 (1998).
10. Britsch, S. *et al.* The transcription factor Sox10 is a key regulator of peripheral glial development. *Genes Dev* **15**, 66-78 (2001).
11. Blair, H.C., Zaidi, M. & Schlesinger, P.H. Mechanisms balancing skeletal matrix synthesis and degradation. *Biochem J* **364**, 329-41 (2002).
12. Yamate, T. *et al.* Osteopontin expression by osteoclast and osteoblast progenitors in the murine bone marrow: demonstration of its requirement for osteoclastogenesis and its increase after ovariectomy. *Endocrinology* **138**, 3047-55 (1997).
13. Millan, J.L. The role of phosphatases in the initiation of skeletal mineralization. *Calcif Tissue Int* **93**, 299-306 (2013).
14. Bianco, P., Silvestrini, G., Termine, J.D. & Bonucci, E. Immunohistochemical localization of osteonectin in developing human and calf bone using monoclonal antibodies. *Calcif Tissue Int* **43**, 155-61 (1988).
15. Michigami, T. Skeletal mineralization: mechanisms and diseases. *Ann Pediatr Endocrinol Metab* **24**, 213-219 (2019).
16. Ponzetti, M. & Rucci, N. Osteoblast Differentiation and Signaling: Established Concepts and Emerging Topics. *Int J Mol Sci* **22**(2021).
17. Hanna, R.M., Ahdoot, R.S., Kalantar-Zadeh, K., Ghobry, L. & Kurtz, I. Calcium Transport in the Kidney and Disease Processes. *Front Endocrinol (Lausanne)* **12**, 762130 (2021).
18. Guo, Y.C. & Yuan, Q. Fibroblast growth factor 23 and bone mineralisation. *Int J Oral Sci* **7**, 8-13 (2015).
19. Areco, V.A., Kohan, R., Talamoni, G., Tolosa de Talamoni, N.G. & Peralta Lopez, M.E. Intestinal Ca(2+) absorption revisited: A molecular and clinical approach. *World J Gastroenterol* **26**, 3344-3364 (2020).
20. Waung, J.A., Bassett, J.H. & Williams, G.R. Thyroid hormone metabolism in skeletal development and adult bone maintenance. *Trends Endocrinol Metab* **23**, 155-62 (2012).
21. Khundmiri, S.J., Murray, R.D. & Lederer, E. PTH and Vitamin D. *Compr Physiol* **6**, 561-601 (2016).
22. Wongdee, K., Rodrat, M., Teerapornpuntakit, J., Krishnamra, N. & Charoenphandhu, N. Factors inhibiting intestinal calcium absorption: hormones and luminal factors that prevent excessive calcium uptake. *J Physiol Sci* **69**, 683-696 (2019).

23. Kovacs, C.S. Bone development and mineral homeostasis in the fetus and neonate: roles of the calciotropic and phosphotropic hormones. *Physiol Rev* **94**, 1143-218 (2014).
24. Lin, C.H. & Hwang, P.P. The Control of Calcium Metabolism in Zebrafish (Danio rerio). *Int J Mol Sci* **17**(2016).
25. Hwang, P.P. & Chou, M.Y. Zebrafish as an animal model to study ion homeostasis. *Pflugers Arch* **465**, 1233-47 (2013).
26. Quinlivan, V.H. & Farber, S.A. Lipid Uptake, Metabolism, and Transport in the Larval Zebrafish. *Front Endocrinol (Lausanne)* **8**, 319 (2017).
27. Fraher, D. *et al.* Zebrafish Embryonic Lipidomic Analysis Reveals that the Yolk Cell Is Metabolically Active in Processing Lipid. *Cell Rep* **14**, 1317-1329 (2016).
28. Miyares, R.L., de Rezende, V.B. & Farber, S.A. Zebrafish yolk lipid processing: a tractable tool for the study of vertebrate lipid transport and metabolism. *Dis Model Mech* **7**, 915-27 (2014).
29. Vanoevelen, J. *et al.* Trpv5/6 is vital for epithelial calcium uptake and bone formation. *FASEB J* **25**, 3197-207 (2011).
30. Xin, Y. *et al.* Cell-autonomous regulation of epithelial cell quiescence by calcium channel Trpv6. *Elife* **8**(2019).
31. Khattar, V., Wang, L. & Peng, J.B. Calcium selective channel TRPV6: Structure, function, and implications in health and disease. *Gene* **817**, 146192 (2022).
32. Fecher-Trost, C. *et al.* Maternal Transient Receptor Potential Vanilloid 6 (Trpv6) Is Involved In Offspring Bone Development. *J Bone Miner Res* **34**, 699-710 (2019).
33. Tseng, D.Y. *et al.* Effects of stanniocalcin 1 on calcium uptake in zebrafish (Danio rerio) embryo. *Am J Physiol Regul Integr Comp Physiol* **296**, R549-57 (2009).
34. Deol, H., Stasko, S.E., De Niu, P., James, K.A. & Wagner, G.F. Post-natal ontogeny of stanniocalcin gene expression in rodent kidney and regulation by dietary calcium and phosphate. *Kidney Int* **60**, 2142-52 (2001).
35. Yeung, B.H., Law, A.Y. & Wong, C.K. Evolution and roles of stanniocalcin. *Mol Cell Endocrinol* **349**, 272-80 (2012).
36. Yoshiko, Y. & Maeda, N. In situ hybridization analysis of stanniocalcin mRNA expressing cells in the mouse kidney. *Mol Cell Endocrinol* **141**, 37-40 (1998).
37. Kobayashi, R. *et al.* Expression of stanniocalcin-1 in gastrointestinal tracts of neonatal and mature rats. *Biochem Biophys Res Commun* **389**, 478-83 (2009).
38. Madsen, K.L. *et al.* Stanniocalcin: a novel protein regulating calcium and phosphate transport across mammalian intestine. *Am J Physiol* **274**, G96-102 (1998).
39. Pang, P.K., Pang, R.K. & Sawyer, W.H. Effects of environmental calcium and replacement therapy on the killifish, Fundulus heteroclitus, after the surgical removal of the corpuscles of Stannius. *Endocrinology* **93**, 705-10 (1973).
40. Naylor, R.W., Chang, H.G., Qubisi, S. & Davidson, A.J. A novel mechanism of gland formation in zebrafish involving transdifferentiation of renal epithelial cells and live cell extrusion. *Elife* **7**(2018).
41. Fenwick, J.C. & So, Y.P. A perfusion study of the effect of stanniectomy on the net influx of calcium 45 across an isolated eel gill (1). *J Exp Zool* **188**, 125-31 (1974).
42. Li, S. *et al.* Calcium State-Dependent Regulation of Epithelial Cell Quiescence by Stanniocalcin 1a. *Front Cell Dev Biol* **9**, 662915 (2021).
43. Oxvig, C. The role of PAPP-A in the IGF system: location, location, location. *J Cell Commun Signal* **9**, 177-87 (2015).
44. Dai, W. *et al.* Calcium deficiency-induced and TRP channel-regulated IGF1R-PI3K-Akt signaling regulates abnormal epithelial cell proliferation. *Cell Death Differ* **21**, 568-81 (2014).
45. Liu, C. *et al.* The metalloproteinase Papp-aa controls epithelial cell quiescence-proliferation transition. *Elife* **9**(2020).

46. Li, S., Li, H., Wang, Z. & Duan, C. Stanniocalcin 1a regulates organismal calcium balance and survival by suppressing Trpv6 expression and inhibiting IGF signaling in zebrafish. *Front Endocrinol (Lausanne)* **14**, 1276348 (2023).
47. Stine, Z.E. *et al.* Oligodendroglial and pan-neural crest expression of Cre recombinase directed by Sox10 enhancer. *Genesis* **47**, 765-70 (2009).
48. Kague, E. *et al.* Skeletogenic fate of zebrafish cranial and trunk neural crest. *PLoS One* **7**, e47394 (2012).
49. Okeke, C. *et al.* Control of cranial ectomesenchyme fate by Nr2f nuclear receptors. *Development* **149**(2022).
50. Kelsh, R.N. *et al.* Zebrafish pigmentation mutations and the processes of neural crest development. *Development* **123**, 369-89 (1996).
51. Malicki, J. *et al.* Mutations affecting development of the zebrafish ear. *Development* **123**, 275-83 (1996).
52. Puchtler, H. & Meloan, S.N. Demonstration of phosphates in calcium deposits: a modification of von Kossa's reaction. *Histochemistry* **56**, 177-85 (1978).
53. Du, S.J., Frenkel, V., Kindschi, G. & Zohar, Y. Visualizing normal and defective bone development in zebrafish embryos using the fluorescent chromophore calcein. *Dev Biol* **238**, 239-46 (2001).
54. Schneider, M.R. Von Kossa and his staining technique. *Histochem Cell Biol* **156**, 523-526 (2021).
55. Teng, C.S. *et al.* Altered bone growth dynamics prefigure craniosynostosis in a zebrafish model of Saethre-Chotzen syndrome. *Elife* **7**(2018).
56. Sim, A.M. *et al.* A novel fluorescein-bisphosphonate based diagnostic tool for the detection of hydroxyapatite in both cell and tissue models. *Sci Rep* **8**, 17360 (2018).
57. Gomez-Picos, P., Ovens, K. & Eames, B.F. Limb Mesoderm and Head Ectomesenchyme Both Express a Core Transcriptional Program During Chondrocyte Differentiation. *Front Cell Dev Biol* **10**, 876825 (2022).
58. Stenzel, A. *et al.* Distinct and redundant roles for zebrafish her genes during mineralization and craniofacial patterning. *Front Endocrinol (Lausanne)* **13**, 1033843 (2022).
59. Barske, L. *et al.* Evolution of vertebrate gill covers via shifts in an ancient Pou3f3 enhancer. *Proc Natl Acad Sci U S A* **117**, 24876-24884 (2020).
60. DeLaurier, A. *et al.* Zebrafish sp7:EGFP: a transgenic for studying otic vesicle formation, skeletogenesis, and bone regeneration. *Genesis* **48**, 505-11 (2010).
61. Apschner, A., Huitema, L.F., Ponsioen, B., Peterson-Maduro, J. & Schulte-Merker, S. Zebrafish enpp1 mutants exhibit pathological mineralization, mimicking features of generalized arterial calcification of infancy (GACI) and pseudoxanthoma elasticum (PXE). *Dis Model Mech* **7**, 811-22 (2014).
62. Huitema, L.F. *et al.* Entpd5 is essential for skeletal mineralization and regulates phosphate homeostasis in zebrafish. *Proc Natl Acad Sci U S A* **109**, 21372-7 (2012).
63. Yadav, M.C. *et al.* Loss of skeletal mineralization by the simultaneous ablation of PHOSPHO1 and alkaline phosphatase function: a unified model of the mechanisms of initiation of skeletal calcification. *J Bone Miner Res* **26**, 286-97 (2011).
64. Christov, M. & Juppner, H. Insights from genetic disorders of phosphate homeostasis. *Semin Nephrol* **33**, 143-57 (2013).
65. Si, J., Wang, C., Zhang, D., Wang, B. & Zhou, Y. Osteopontin in Bone Metabolism and Bone Diseases. *Med Sci Monit* **26**, e919159 (2020).
66. Suarez-Bregua, P. *et al.* Pth4, an ancient parathyroid hormone lost in eutherian mammals, reveals a new brain-to-bone signaling pathway. *FASEB J* **31**, 569-583 (2017).
67. Pan, T.C., Liao, B.K., Huang, C.J., Lin, L.Y. & Hwang, P.P. Epithelial Ca(2+) channel expression and Ca(2+) uptake in developing zebrafish. *Am J Physiol Regul Integr Comp Physiol* **289**, R1202-11 (2005).

68. Rozycka, M.O. *et al.* Effect of Gel Exposition on Calcium and Carbonate Ions Determines the Stm-I Effect on the Crystal Morphology of Calcium Carbonate. *Biomacromolecules* **24**, 4042-4050 (2023).
69. Lundberg, Y.W., Xu, Y., Thiessen, K.D. & Kramer, K.L. Mechanisms of otoconia and otolith development. *Dev Dyn* **244**, 239-53 (2015).
70. Huitema, L.F. *et al.* Macrophage-stimulating protein and calcium homeostasis in zebrafish. *FASEB J* **26**, 4092-101 (2012).
71. Dymowska, A.K., Hwang, P.P. & Goss, G.G. Structure and function of ionocytes in the freshwater fish gill. *Respir Physiol Neurobiol* **184**, 282-92 (2012).
72. Dai, W. *et al.* Duplicated zebrafish insulin-like growth factor binding protein-5 genes with split functional domains: evidence for evolutionarily conserved IGF binding, nuclear localization, and transactivation activity. *FASEB J* **24**, 2020-9 (2010).
73. Janicke, M., Carney, T.J. & Hammerschmidt, M. Foxi3 transcription factors and Notch signaling control the formation of skin ionocytes from epidermal precursors of the zebrafish embryo. *Dev Biol* **307**, 258-71 (2007).
74. Sur, A. *et al.* Single-cell analysis of shared signatures and transcriptional diversity during zebrafish development. *Dev Cell* **58**, 3028-3047 e12 (2023).
75. Kwong, R.W., Auprix, D. & Perry, S.F. Involvement of the calcium-sensing receptor in calcium homeostasis in larval zebrafish exposed to low environmental calcium. *Am J Physiol Regul Integr Comp Physiol* **306**, R211-21 (2014).
76. Radman, D.P., McCudden, C., James, K., Nemeth, E.M. & Wagner, G.F. Evidence for calcium-sensing receptor mediated stanniocalcin secretion in fish. *Mol Cell Endocrinol* **186**, 111-9 (2002).
77. Lin, C.H., Hu, H.J. & Hwang, P.P. Molecular Physiology of the Hypocalcemic Action of Fibroblast Growth Factor 23 in Zebrafish (Danio rerio). *Endocrinology* **158**, 1347-1358 (2017).
78. Lin, C.H., Su, C.H. & Hwang, P.P. Calcium-sensing receptor mediates Ca(2+) homeostasis by modulating expression of PTH and stanniocalcin. *Endocrinology* **155**, 56-67 (2014).
79. Wendelaar Bonga, S.E., Greven, J.A. & Veenhuis, M. Vascularization, innervation, and ultrastructure of the endocrine cell types of stannius corpuscles in the teleost Gasterosteus aculeatus. *J Morphol* **153**, 225-43 (1977).
80. Cheng, C.N. & Wingert, R.A. Nephron proximal tubule patterning and corpuscles of Stannius formation are regulated by the sim1a transcription factor and retinoic acid in zebrafish. *Dev Biol* **399**, 100-116 (2015).
81. Naylor, R.W. *et al.* BMP and retinoic acid regulate anterior-posterior patterning of the non-axial mesoderm across the dorsal-ventral axis. *Nat Commun* **7**, 12197 (2016).
82. Kobayashi, I. *et al.* Jam1a-Jam2a interactions regulate haematopoietic stem cell fate through Notch signalling. *Nature* **512**, 319-23 (2014).
83. Das, A. & Crump, J.G. Bmps and id2a act upstream of Twist1 to restrict ectomesenchyme potential of the cranial neural crest. *PLoS Genet* **8**, e1002710 (2012).
84. Ninov, N., Borius, M. & Stainier, D.Y. Different levels of Notch signaling regulate quiescence, renewal and differentiation in pancreatic endocrine progenitors. *Development* **139**, 1557-67 (2012).
85. Kraus, J.M. *et al.* Notch signaling enhances bone regeneration in the zebrafish mandible. *Development* **149**(2022).
86. Carney, T.J. *et al.* A direct role for Sox10 in specification of neural crest-derived sensory neurons. *Development* **133**, 4619-30 (2006).
87. Meloan SNP, H. Chemical Mechanisms of staining methods: Von Kossa's technique: what von Kossa really wrote and a modified reaction for selective demonstration of inorganic phosphates. *J Histotechnol* **8**(185).

88. Santos, J.M.A., Laize, V., Gavaia, P.J., Conceicao, N. & Cancela, M.L. Zebrafish Models to Study Ectopic Calcification and Calcium-Associated Pathologies. *Int J Mol Sci* **24**(2023).
89. Lin CH, L., S. T., Wang, Y. C., Tsou, Y. L. & Hu, H. J. Vitamin D regulates transepithelial acid secretion in zebrafish (Danio rerio) larvae. *Front Mar Sci* **9**(2022).
90. Lin, C.H., Su, C.H., Tseng, D.Y., Ding, F.C. & Hwang, P.P. Action of vitamin D and the receptor, VDRa, in calcium handling in zebrafish (Danio rerio). *PLoS One* **7**, e45650 (2012).
91. Hogan, B.M. *et al.* Duplicate zebrafish pth genes are expressed along the lateral line and in the central nervous system during embryogenesis. *Endocrinology* **146**, 547-51 (2005).
92. Guerrera, M.C., De Pasquale, F., Muglia, U. & Caruso, G. Digestive enzymatic activity during ontogenetic development in zebrafish (Danio rerio). *J Exp Zool B Mol Dev Evol* **324**, 699-706 (2015).
93. Elizondo, M.R., Budi, E.H. & Parichy, D.M. trpm7 regulation of in vivo cation homeostasis and kidney function involves stanniocalcin 1 and fgf23. *Endocrinology* **151**, 5700-9 (2010).
94. Mangos, S. *et al.* Expression of fgf23 and alphaklotho in developing embryonic tissues and adult kidney of the zebrafish, Danio rerio. *Nephrol Dial Transplant* **27**, 4314-22 (2012).
95. Martinez-Heredia, L., Canelo-Moreno, J.M., Garcia-Fontana, B. & Munoz-Torres, M. Non-Classical Effects of FGF23: Molecular and Clinical Features. *Int J Mol Sci* **25**(2024).
96. Rodrat, M. *et al.* Modulation of fibroblast growth factor-23 expression and transepithelial calcium absorption in Caco-2 monolayer by calcium-sensing receptor and calcineurin under calcium hyperabsorptive state. *Biochem Biophys Res Commun* **659**, 105-112 (2023).
97. Drummond, B.E., Li, Y., Marra, A.N., Cheng, C.N. & Wingert, R.A. The tbx2a/b transcription factors direct pronephros segmentation and corpuscle of Stannius formation in zebrafish. *Dev Biol* **421**, 52-66 (2017).
98. Krishnamurthy, V.G. & Bern, H.A. Innervation of the corpuscles of Stannius. *Gen Comp Endocrinol* **16**, 162-5 (1971).
99. Kamenev, D. *et al.* Schwann cell precursors generate sympathoadrenal system during zebrafish development. *J Neurosci Res* **99**, 2540-2557 (2021).
100. An, M., Luo, R. & Henion, P.D. Differentiation and maturation of zebrafish dorsal root and sympathetic ganglion neurons. *J Comp Neurol* **446**, 267-75 (2002).
101. Vega-Lopez, G.A., Cerrizuela, S., Tribulo, C. & Aybar, M.J. Neurocristopathies: New insights 150 years after the neural crest discovery. *Dev Biol* **444 Suppl 1**, S110-S143 (2018).
102. M., W. *The zebrafish book. A guide for the laboratory use of zebrafish (Danio rerio.*, (University of Oregon Press, Eugene, 2007).
103. Lawson, N.D. & Weinstein, B.M. In vivo imaging of embryonic vascular development using transgenic zebrafish. *Dev Biol* **248**, 307-18 (2002).
104. Jiang, Y. *et al.* Glucocorticoids induce osteoporosis mediated by glucocorticoid receptor-dependent and -independent pathways. *Biomed Pharmacother* **125**, 109979 (2020).
105. Walker, M.B. & Kimmel, C.B. A two-color acid-free cartilage and bone stain for zebrafish larvae. *Biotech Histochem* **82**, 23-8 (2007).
106. Paese CLB, C., C. F., Kristeková, D. & Brugmann. Pharmacological intervention of the FGF–PTH axis as a potential therapeutic for craniofacial ciliopathies. Disease. *Disease Models and Mechanisms* **15**(2022).
107. Khrystoforova, I. *et al.* Zebrafish mutants reveal unexpected role of Lrp5 in osteoclast regulation. *Front Endocrinol (Lausanne)* **13**, 985304 (2022).
108. Paul, S. *et al.* Ihha induces hybrid cartilage-bone cells during zebrafish jawbone regeneration. *Development* **143**, 2066-76 (2016).
109. Barske, L. *et al.* Essential Role of Nr2f Nuclear Receptors in Patterning the Vertebrate Upper Jaw. *Dev Cell* **44**, 337-347 e5 (2018).

Figures

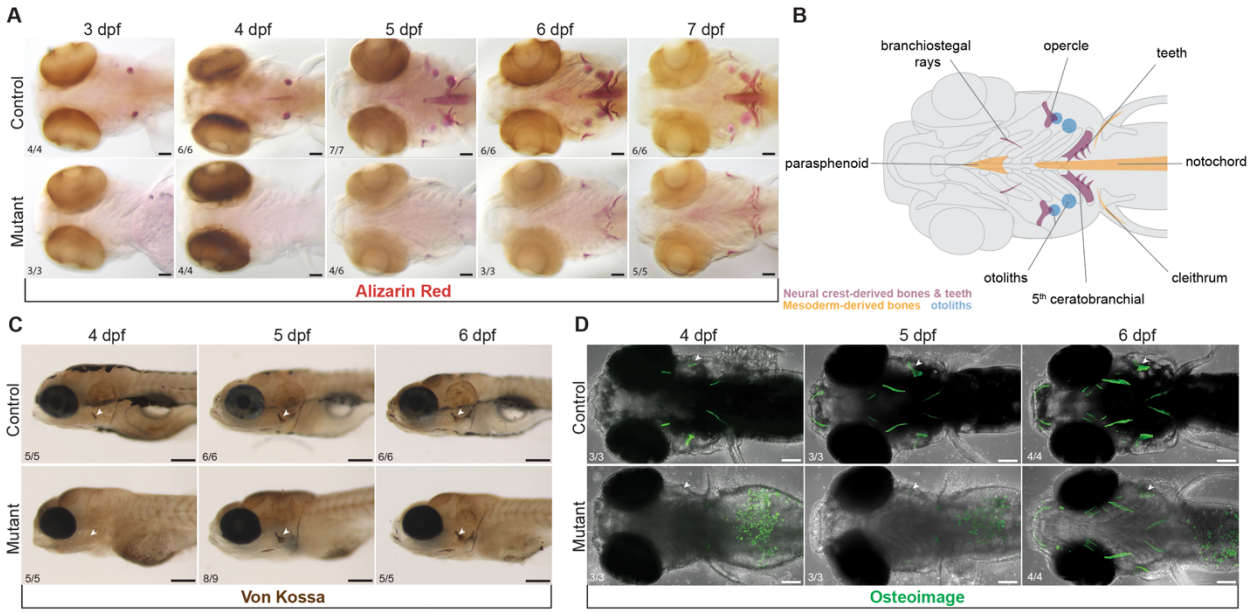

Figure 1. Mineralization deficit in zebrafish *sox10* mutants. (A) A major delay in initiation of bone mineralization in *sox10* mutants between 3 and 7 dpf is revealed by Alizarin red staining. Some mineralization is present by 5 dpf but never achieves control levels before lethality at 8 dpf. Scale bar: 100 μm. Schematic representation of the affected mineralized structures and their embryonic origins. **(C, D)** Von Kossa (C, scale bar: 200 μm), and Osteoimage (D, scale bar: 100 μm) staining show absent calcium deposition and hydroxyapatite formation in *sox10* mutants at 4 dpf and gradual recovery starting at 5 dpf. Arrowheads pointing at the opercle (op). Numbers in all panels indicate the proportion of larvae of that genotype with the presented phenotype.

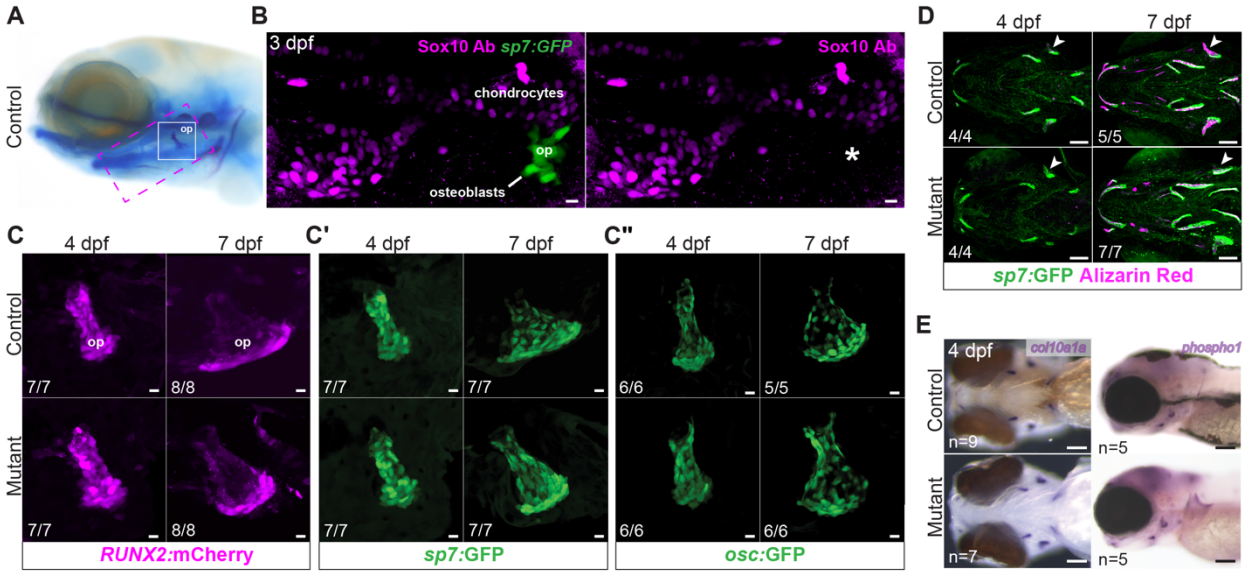

781

782 **Figure 2. Normal patterns of growth and differentiation in *sox10* mutant osteoblasts. (A)**
783 Reference image of a larva stained with Alcian blue and Alizarin red, with locations of skeletal
784 elements shown in B (magenta dashed line) and C (white line) highlighted. op, opercle. **(B)**
785 Immunostaining with an anti-Sox10 antibody reveals strong expression in chondrocytes but a lack
786 of Sox10 protein (asterisk) in mineralizing osteoblasts (*sp7*:GFP+) forming the op bone at 3 dpf.
787 Scale bar: 10 μm. **(C)** Normal growth of *sox10* mutant op (arrowhead) as well as other bones
788 despite minimal calcium accumulation, revealed by live imaging of Alizarin red-stained *sp7*:GFP+
789 embryos at 4 and 7 dpf. Scale bar: 100 μm. **(D-D")** Sequential live imaging shows normal patterns
790 of *RUNX2*:mCherry, *sp7*:GFP and *osc*:GFP transgene expression in mutant osteoblasts of the op
791 at 4 and 7 dpf. Scale bar: 10 μm. **(E)** Colorimetric *in situ* hybridizations for *col10a1a* and *phospho1*,
792 encoding key bone matrix components, revealed no overt abnormalities in *sox10* mutants at 4
793 dpf. Scale bar: 100 μm.

794

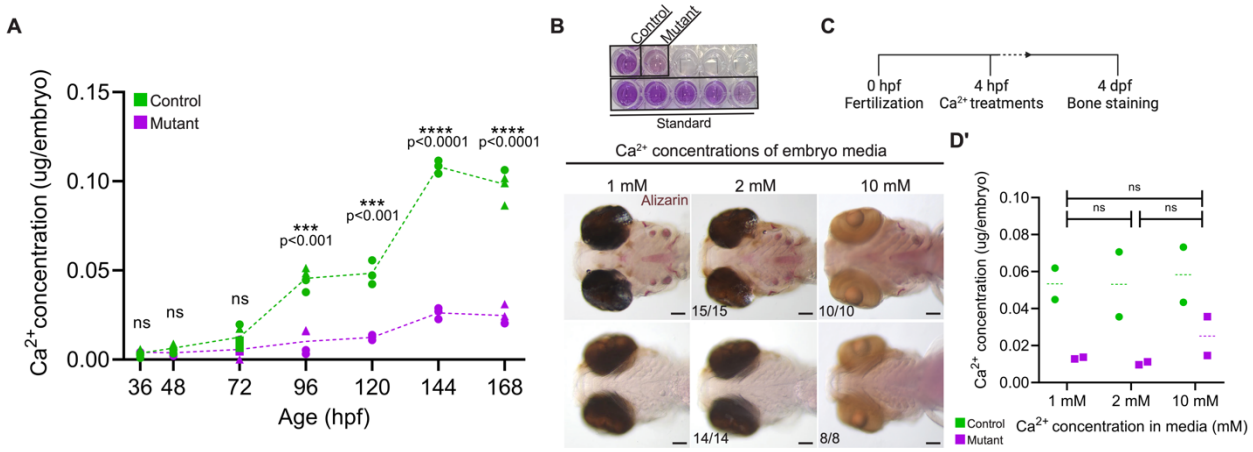

795

796 **Figure 3. *sox10* mutants have a severe whole-body calcium deficit. (A-B)** Colorimetric
797 calcium assay reveals significantly lower levels of Ca^{2+} in *sox10* mutants after mineralization is
798 initiated at 3 dpf. Each data point represents a pool of 10-15 embryos. Different shapes represent
799 biological replicates assayed on different days (unpaired t-tests: 36 hpf: p=0.580, df=8; 48 hpf:
800 p=0.083, df=8; 72 hpf: p=0.091, df=7; 96 hpf: p=0.0002, df=6; 120 hpf: p=0.0008, df=4; 144 hpf:
801 p=0.000008, df=4; 168 hpf: p=0.000005, df=6). B is an example of the colorimetric assay, showing
802 a clear reduction in mutants. **(C)** Schematic representation of the Ca^{2+} treatment protocol. **(D-D')**
803 Increasing ambient Ca^{2+} levels to 2 or 10 mM does not rescue the mineralization deficit (D; scale
804 bar: 100 μm) or Ca^{2+} content (D') (unpaired t-tests: 1 vs. 2 mM: p=0.963, df=2; 1 vs. 10 mM:
805 p=0.778, df=2; 2 vs. 10 mM: p=0.748, df=2). Ratios reflect the number of imaged larvae of that
806 genotype with the presented phenotype. In D', bars indicate the median; significance determined
807 by unpaired t-test. Scale bar: 100 μm.

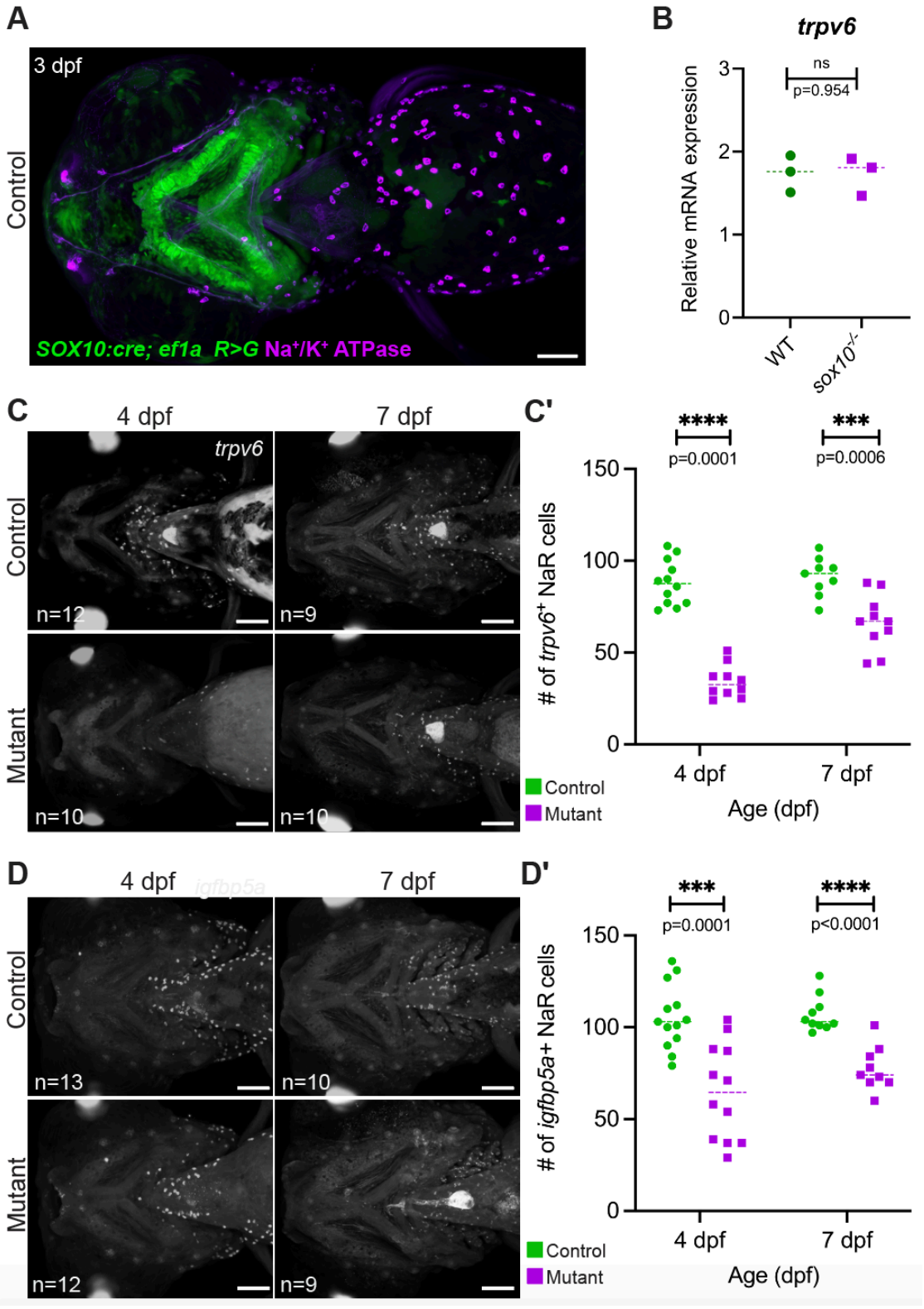

Figure 4. Reduction in *trpv6*+ NaR cell number in the *sox10* mutants. (A) Immunostaining of a 3 dpf *SOX10:Cre; ef1a: DsRed>GFP* larva with an antibody against the Na+/K+ ATPase pump

confirms that NaR ionocytes do not derive from neural crest. Scale bar: 100 μm. **(B)** rt-PCR demonstrates that *trpv6* transcription is not overtly altered at the whole-body level at 4 dpf. Each point represents a pool of 10-15 embryos (unpaired t-test: p=0.954, df=4). **(C-D')** Fluorescent *in situ* hybridizations for *igfbp5a* and *trpv6* (C,D) both demonstrate a striking and significant reduction in the number of NaR cells in mutants at 4 dpf (quantified in C', D'), with partial recovery by 7 dpf (unpaired t-tests; *trpv6*: 4 dpf: p<0.000001, df=20; 7 dpf: p=0.0006, df=17; *igfbp5a:* 4 dpf: p=0.0001, df=23; 7 dpf: p<0.0001, df=17). Scale bar: 100 μm.

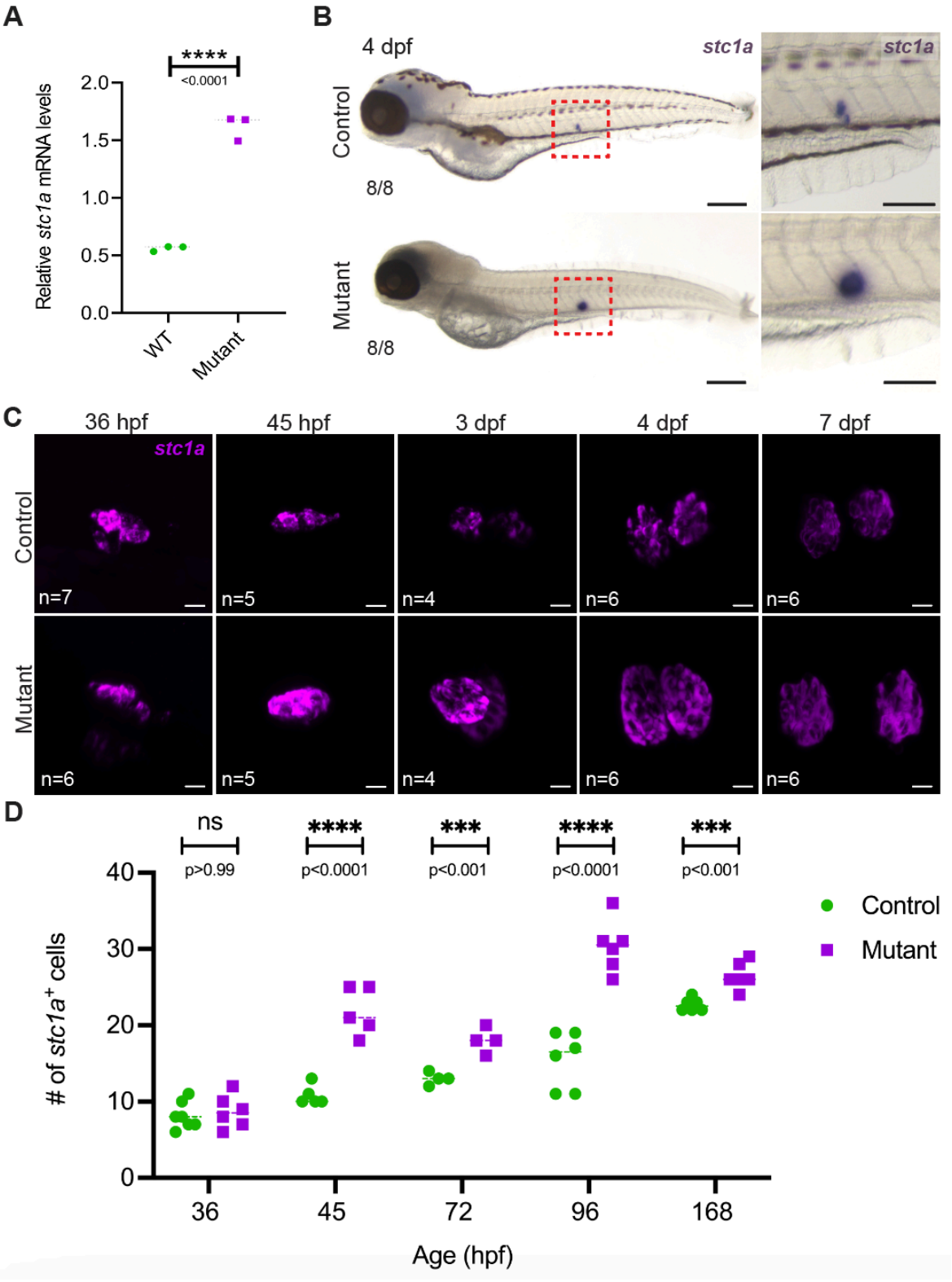

Figure 5. Upregulation of anti-hypercalcemic hormone *stc1a* in *sox10* mutants. (A-B) Both semi-quantitative rt-PCR (A) and *in situ* hybridization (B) detect a robust upregulation of *stc1a*

822 mRNA in *sox10* mutants at 4 dpf (unpaired t-test in A, $p<0.0001$, $df=4$). Scale bars: 200 μm in B
823 and 100 μm in inset. (C-D) The increase in *stc1a* transcript levels is due at least in part to an
824 increase in the number of *stc1a*+ cells in *sox10* mutant Corpuscles, first detected at 45 hpf and
825 resolving at 7 dpf (unpaired t-tests; 36 hpf: $p=0.640$, $df=11$; for 45 hpf: $p=0.00009$, for $df=8$; for 72
826 hpf: $p=0.002$, $df=6$; for 96 hpf: $p=0.00003$, $df=10$; for 168 hpf: $p=0.0007$, $df=10$. Scale bars in C:
827 10 μm.
828

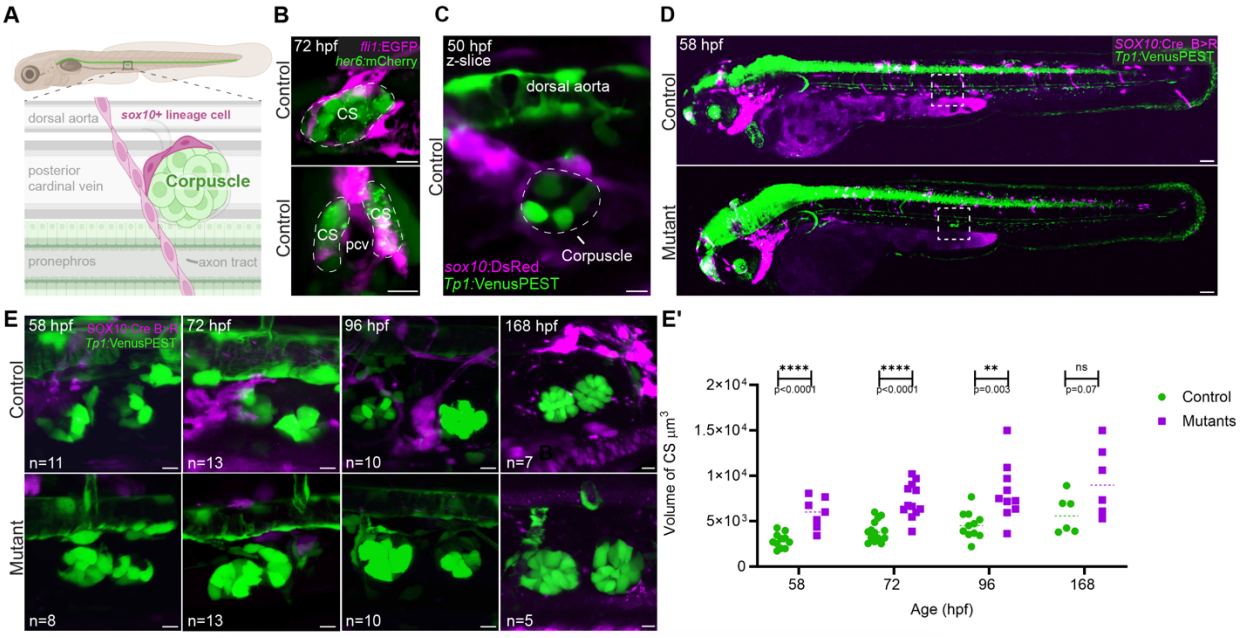

Figure 6. *sox10*+ crest-derived cells surround the Corpuscles of Stannius and are missing in *sox10* mutants. (A) Schematic representation of the Corpuscles' position and surrounding environs. The glands are positioned ventral to the dorsal aorta (da), dorsal to the pronephros, and flanking the posterior cardinal vein (pcv). *sox10*+ lineage cells branch off neighboring axon tracts (lined with sox10+ Schwann cells and Schwann cell precursors) to contact the Corpuscles. **(B)** Control 72 hpf larva doubly transgenic for *fli1:*EGFP (magenta, labeling vasculature) and *her6:*mCherry (green, labeling the Corpuscles). Top image is a single optical section from the lateral perspective showing endothelial cells wrapping around the CS. Bottom image is a maximum intensity projection rotated orthogonally to show the close interaction of the CS with the pcv. **(C)** Single optical section showing that *sox10:*DsRed+ cells are also in close contact with the *Tp1*:VenusPEST+ Corpuscles by 50 hpf. **(D-E)** Whole-mount live imaging of *SOX10:Cre B>R; Tp1*:VenusPEST fish shows *sox10*+ lineage cells surrounding the CS at earlier stages (58 and 72 hpf), nearby at 96 and 168 hpf, and absent in the *sox10* mutants. The entire fish is shown in D to highlight the deficiency of trunk NCCs (magenta). **(E')** Volume measurements of control and mutant *Tp1:*VenusPEST+ CS between 58 and 168 hpf. Only the right CS, closest to the lens, was

845 measured (unpaired t-tests; 58 hpf: p=0.0001, df=16; 72 hpf: p=0.00001, df=24; 96 hpf: p=0.003,

846 df=19; 168 hpf: p=0.068, df=10). Scale bars: B and D: 10 μm, C: 100 μm.

847

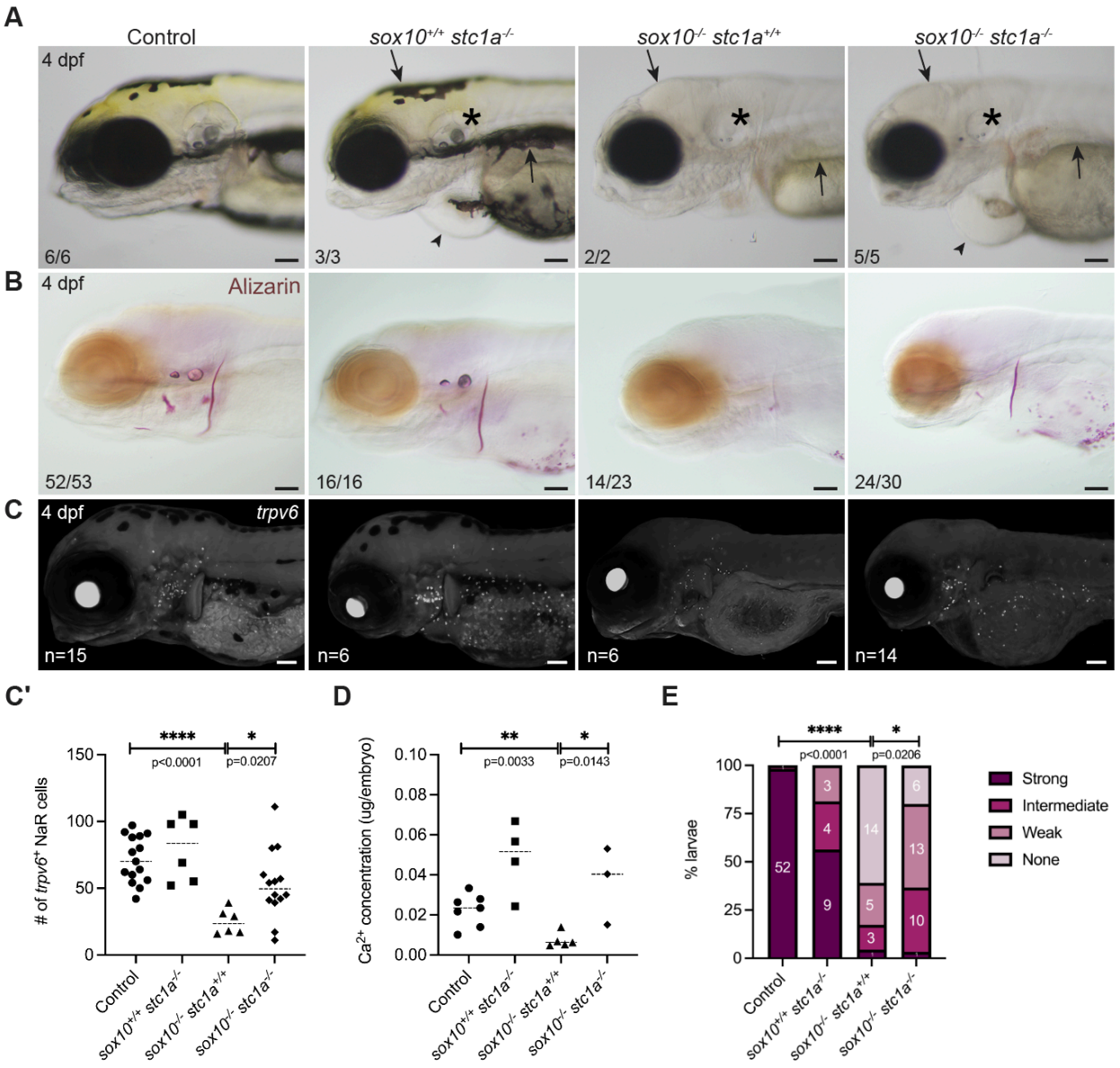

Figure 7. *stc1a* is epistatic to *sox10* in control of systemic calcium content. **(A)** Brightfield images of *sox10* and *stc1a* controls and mutants at 4 dpf. Double mutants phenocopy the loss of pigment (arrow) and the inner ear malformations (asterisk) of single *sox10* mutants and the cardiac edema of the *stc1a* mutant (arrowhead). **(B-C')** Loss of *stc1a* on the *sox10* mutant background improves mineralization **(B)** and the number of *trpv6*+ ionocytes **(C)** at 4 dpf, quantified in C' (unpaired t-test; p=0.0207, df=18). Dashed bars indicate the median. **(D)** Calcium quantification shows an increase (unpaired t-test; p=0.143, df=6) in calcium levels in *sox10*$^{-/-}$;

856 *stc1a*$^{-/-}$ compared to *sox10*$^{-/-}$. Dashed bars indicate the median. **(E)** Quantitation of mineralization
857 levels in *sox10; stc1a* clutches grouped based on the intensity of the Alizarin red staining. There
858 was a significant increase in the proportion of double mutants with detectable mineralization
859 compared with *sox10* single mutants (Chi-square; p=0.0206, df=3). In C'-E, 'control' includes wild-
860 type and heterozygous larvae. Scale bars: 100 μm.